AD-758 133

NONCRYSTALLINE SEMICONDUCTORS: ELECTRICAL AND THERMAL PROCESSES

Lyle H. Slack

Virginia Polytechnic Institute

Prepared for:

Advanced Research Projects Agency

28 February 1973

DISTRIBUTED BY:

NTIS

National Technical Information Service
U. S. DEPARTMENT OF COMMERCE
5285 Port Royal Road, Springfield Va. 22151

Virginia Polytechnic Institute
& State Univ., Blacksburg

Annual Technical Report

AD758133

Title: Noncrystalline Semiconductors: Electrical and Thermal Processes

ARPA Order No. 1562, Amend No. 1

Grant No. DA-ARO-D-31-124-72-G72

Program Code No. 61101D

Principal Investigator and Project Scientist:

Lyle H. Slack
(703) 552-6777

Effective Date of Grant: 1 January 1972

Expiration Date: 31 December 1973

Date of Report: February 28, 1973

Amount of Grant: $40,000

The views and conclusions contained in this document are those of the author and should not be interpreted as necessarily representing the official policies, either expressed or implied, of the Advanced Research Projects Agency of the U. S. Government.

Sponsored by

Advanced Research Projects Agency
ARPA Order No. 1562, Amen No. 1.

Monitored by

U. S. Army Research Office - Durham

Approved for public release;
distribution unlimited.

Reproduced by
NATIONAL TECHNICAL
INFORMATION SERVICE
U S Department of Commerce
Springfield VA 22151

DDC
RECEIVED
APR 6 1973
B

43

Table of Contents

Preface ii

Part I. Experimental and Computer Studies of Switching in AsTe Films

A. Introduction 1

B. Procedure 1

1. Sample Preparation 1
2. Electrical Measurements 3
3. Scanning Electron Microscopy 5
4. Computer Simulation 6

C. Results 7

D. Discussion 16

E. Summary and Conclusions 17

F. Future Work 17

Part II. Electron Spectra of Crystalline and Amorphous Si, Ge, and AsTe.

A. Introduction 19

B. Experimental 22

C. Results and Discussion 23

1. Subvalence Levels of Ge and Si 23
2. Valence Electron Spectra of Ge and Si 26
3. Subvalence Electron Levels of Te 29
4. Valence Electron Levels of AsTe 31

D. Interpretation and Results 34

E. Conclusions 37

F. Future Work 37

References 38

Details of illustrations in this document may be better studied on microfiche

Annual Technical Report

AMORPHOUS SEMICONDUCTORS: ELECTRICAL AND THERMAL PROCESSES

The purpose of this research project is to characterize the switching process in selected amorphous semiconductors. The research has been divided into two parts, the first comparing the actual switching behavior of amorphous semiconductor films with computer simulations of switching based on an assumed thermal model. The second part of the research compares the electron energy spectrum of crystalline and amorphous semiconductors of the same composition in order to understand the uniqueness of the amorphous semiconductor's electrical properties. Each of these parts is associated with the graduate research assistants, Mr. W. D. Leahy and Mr. L. R. Durden.

One paper[43] has been published based in part on research supported by this grant. It is entitled "Pre-Switching and Post-Switching Phenomena in Amorphous Semiconducting Films." This research indicates that the switching consists of a filament forming process, this filamentary volume within the film being the preferred site for subsequent switching events.

Part I

EXPERIMENTAL AND COMPUTER STUDIES OF SWITCHING IN AsTe FILMS

A. Introduction

The objective of this portion of the project is to compare the actual switching behavior of amorphous semiconductor thin films with computer simulations of switching based on an assumed thermal mechanism. Switching has been studied and good agreement between experimental and simulated data has been observed. Oscillations similar to those reported by Haden et al.[1] were not observed in this study. Relatively slow Joule heating was observed. However, threshold switching appears to be due to Joule heating in a very small area, this area being selected by some undetermined process.

B. Procedure

1. Sample Preparation

A top view of a typical substrate used in the experimental work is shown in Figure 1. The fabrication procedure was as follows: Aluminum disks were polished through .05 μm MgO and coated with a thin film of molybdenum. A thin film of AsTe was R.F. sputtered[A] onto the molybdenum surface producing a good thermal and electrical contact with a minimum probability of diffusion. Photoresist[B] was applied to the AsTe surface by spraying and baking at 60°C. A glass photo mask[C] with a 5 by 5 matrix of dots (50, 100, 200, 400, and

---

[A] R. D. Mathis SP-310A.

[B] For a general discussion of Photolithography, see L. I. Maissel and R. Glang, "Handbook of Thin Film Technology," Chap. 7, McGraw-Hill, 1970.

[C] Fabricated to order by Towne Laboratories, Inc., Somerville, N. J. 08876.

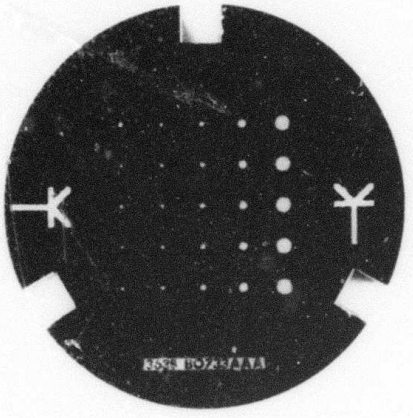

Figure 1. Substrate with twenty-five devices, as fabricated.

800 μm in diameter) was aligned onto the substrate and the photoresist exposed to ultraviolet light. The photoresist was then developed and a metal shadow mask[C] aligned onto the substrate. A molybdenum spot was then deposited over each hole in the photoresist followed by a similar deposit of aluminum. Unlike most conventional techniques, the photoresist is not removed; instead, it is left in place to act as a dielectric. The finished device consists of a circular spot of AsTe thin film, contacted on both sides with a Mo film.

2. Electrical Measurements

A schematic drawing of the experimental circuit is shown in Figure 2. In order to minimize spurious electrical effects such as "ringing", and to facilitate proper probe alignment, a special test stand was designed. The stand consisted of an aluminum block recessed to hold the sample and a limiting resistor (R_L). The block rested on a copper clad printed circuit board, copper side down. The ground lead of the limiting resistor passed through the board and was soldered to the copper ground plane. An oscilloscope probe was inserted into a hole drilled in the aluminum block and a pulse generator connected the test stand via type N coaxial cable with an adapter connecting the cable to a flange mount terminal. A short piece of wire was soldered into the center contact to act as a probe. A 50 ohm terminating resistor (R_T) was soldered between the center contact and the flange. A braided strap connected the flange, the ground plane, and the ground on the oscilloscope probe.

A microscope was modified to allow for correct positioning of the contact probe and sample by replacing the optics with a holder for the

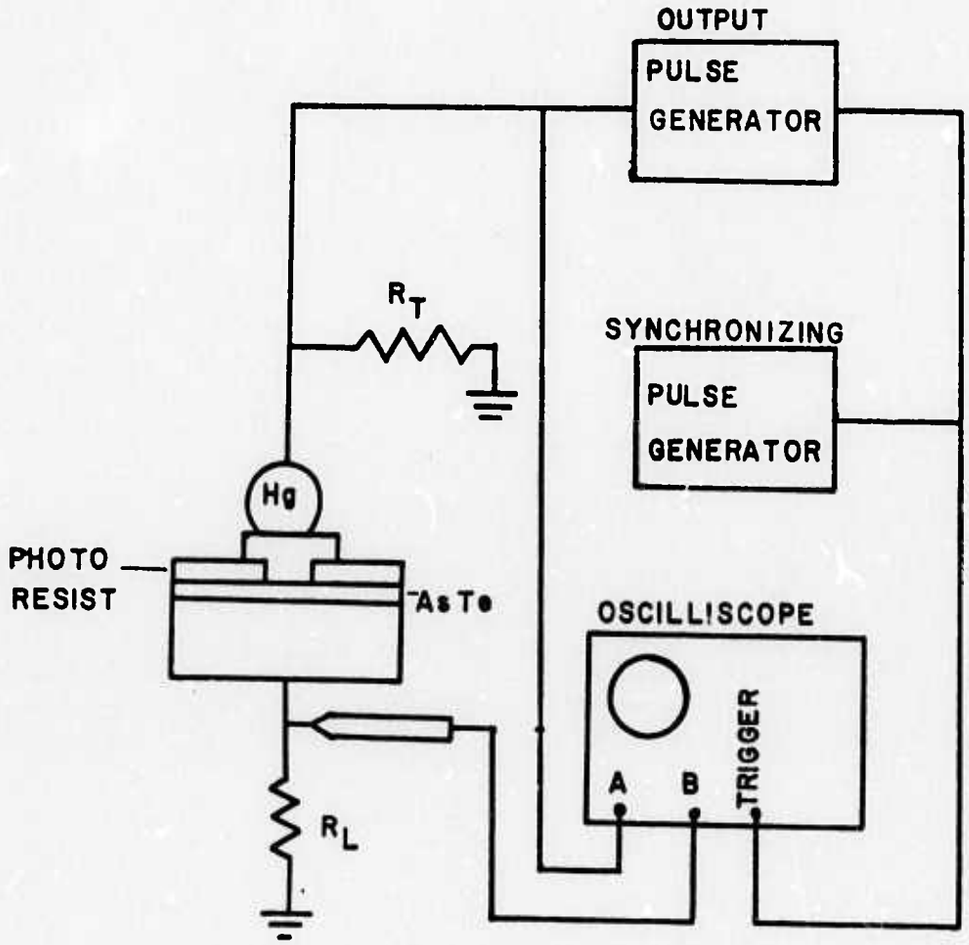

Figure 2. Schematic of experimental test circuit.

contact probe. This allowed both coarse and fine vertical movement of the probe. The previously described sample holder was mounted on the microscope's mechanical stage, permitting fine movement in the horizontal x and y directions. Positioning of the probe with respect to the sample was observed through an obliquely mounted binocular zoom microscope.

A mercury ball, approximately the same size as the device to be tested, was positioned on the device and the probe lowered until contact was made. This kind of mercury contact insures good electrical and thermal contact between the device and the probe.

A synchronizing pulse generator[D] (typical frequency 1 kHz) triggered the output generator[E] and oscilloscope[F]. The applied voltage pulse and the voltage across the limiting resistor were observed on the oscilloscope. The amplitude of the applied voltage was increased until either stable switching or device failure occurred. The oscillographs of unstable devices were obtained using time exposures while those of the stable device were obtained using multiple exposures.

3. Scanning Electron Microscopy

After completing electrical measurements, each device was microscopically examined using a scanning electron microscope[G] (SEM) operating at 20 kV.

[D] General Radio Type 1217-B.

[E] Hewlett Packard Model 212A

[F] Tektronix 7904 with 7A19 and 7B53 plug-in units.

[G] AMR 900.

To eliminate charging effects from the photoresist, each substrate was coated with 200 to 250 Å of Au-Pd. No attempt was made to remove the top electrode since the purpose of the SEM study was to determine the failure mechanism.

4. Computer Simulation

Computer simulation of thermal switching consists basically of performing a set of operations N times, where:

$$N = \frac{\text{Pulse Duration}}{\text{Selected Time Increment}} .$$

Assuming initial temperature, device geometry, and material and electrical parameters are known, the operations are as follows:

a. Calculate the resistivity as a function of temperature, using the appropriate Arrhenius equation

$$\rho = \rho_o \exp(E/2kT)$$

where ρ_o and E are experimentally determined material parameters.

b. Calculate the device's resistance from the resistivity, film thickness, and filament radius

$$R_D = \rho \cdot \frac{t}{A}$$

where t is the film thickness and A the filamentary cross-sectional area.

c. Calculate the current through the device using ohms law

$$I = V/(R_D + R_L)$$

where V is the applied voltage and R_L is the limiting resistor.

d. Calculate the amount of joule heating from the current and time increment

$$\Delta Q = I^2 R .$$

e. Calculate the increase in temperature

$$\Delta T = \frac{\Delta Q}{CdV}$$

where C is the heat capacity, d the density, and V the volume of the filament.

f. Repeat steps 1 through 5, N times.

On each pass through the simulation, the values of current and temperature are produced as output, usually in the form of a plot. The simulation is useful both in determining what effect changing different parameters will have on the switching characteristics and in interpreting the various phenomena observed during the experimental work.

C. Results

Typical waveforms of a device exhibiting stable switching are shown in Figure 3. The top set of traces represent the applied voltage pulses while the bottom set represent the current through the device (actually, the voltage across the limiting resistor). In addition to the stable devices observed, a great number of unstable devices were found. The waveforms of such a device are shown in Figure 4. This photograph was made using a 1 to 2 second time exposure.

The delay time before switching is given by Sugi[2] as

$$t_d = \left(\frac{A}{V-V_o}\right)^2$$

where A and V_o are empirical constants and V is the applied voltage.

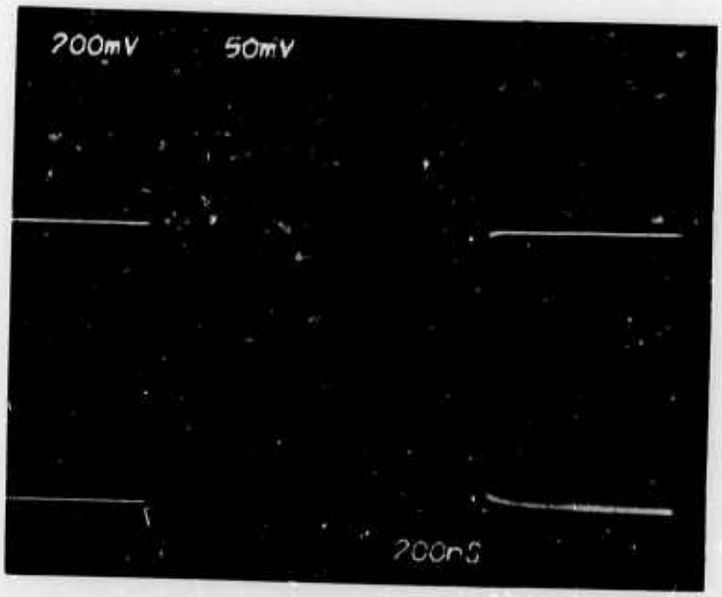

Figure 3. Typical stable switching.

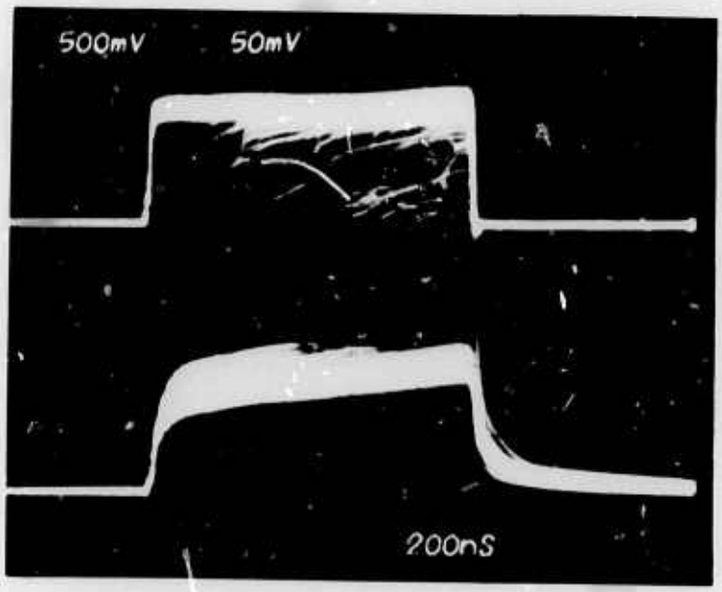

Figure 4. Typical unstable switching.

This relationship is shown in Figure 5 for the AsTe films. The solid line is a least squares fit to the experimental data intersecting the voltage axis at V_o, the theoretical minimum voltage below which switching will not occur over an infinite time. The dashed line represents computer simulated data. Contrary to the experimental data, the computer simulation intersects the origin. Since cooling is neglected, simulated switching can occur at any positive voltage given sufficient time. In actual devices, cooling becomes appreciable at lower voltages and long pulse times.

The effect of filament radius and film thickness on switching characteristics was studied using the computer (Figures 6 and 7). Table I is the data obtained from the simulation shown in Figure 6. The switching delay time, t_d, is thickness dependent, but the rate of current rise is not. This current rise is, however, very dependent on the radius of the heated region. With these two relations in mind, excellent agreement between the actual experimental data (Figure 3) and the simulated experimental data (Figure 8) was obtained using an optimum simulated filament radius of 3μ.

The Scanning Electron Microscope revealed different surface characteristics for different kinds of devices. Stable devices were generally smooth with occasional regions of "pinholing" (Figures 9 and 10). On the other hand, unstable devices and burned out devices showed a more pronounced degree of "pinholing" to the point where portions of the top electrode seem to be missing (Figures 11 and 12).

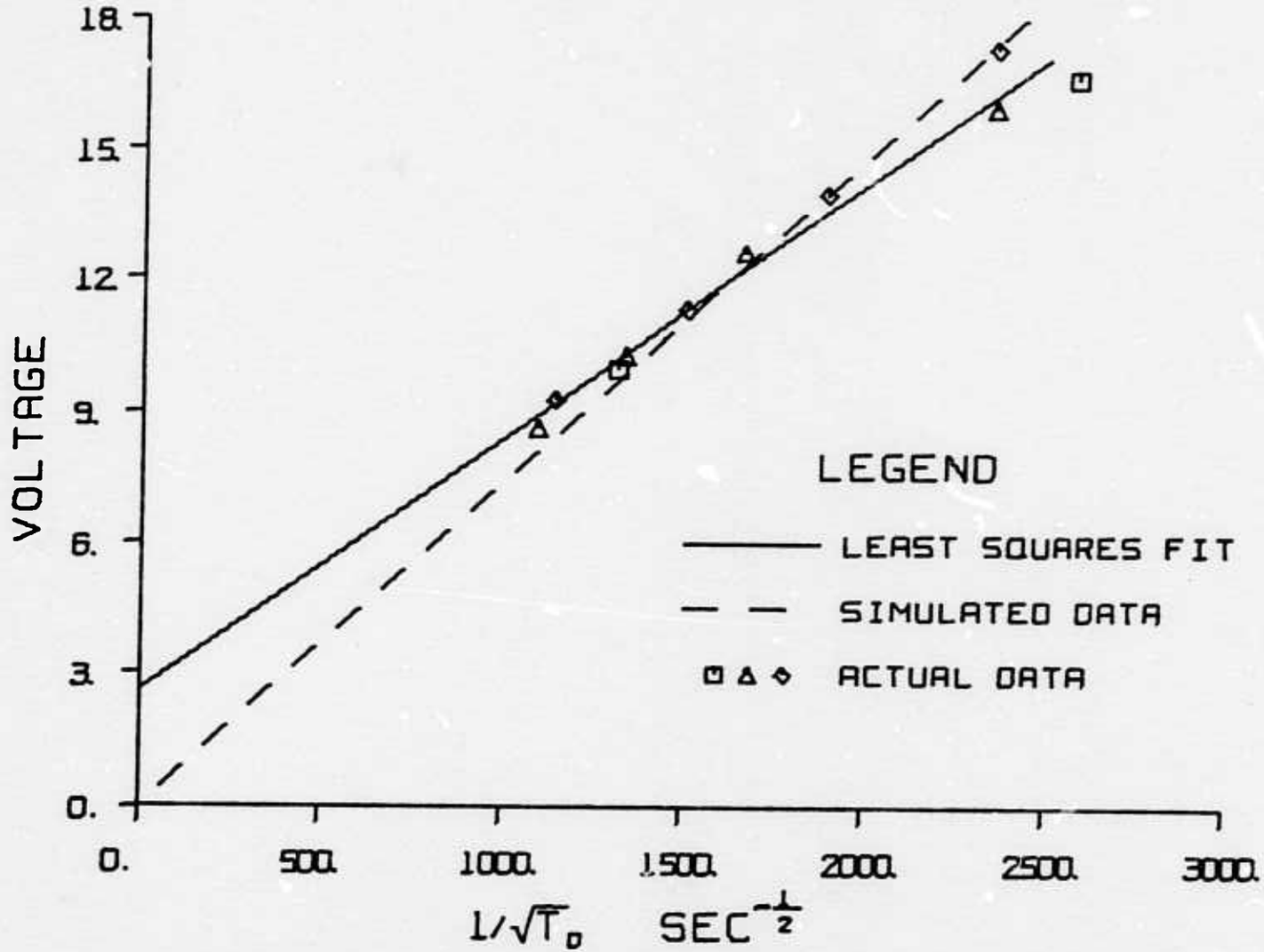

Figure 5. Voltage vs. square root of 1/T, simulated and actual data.

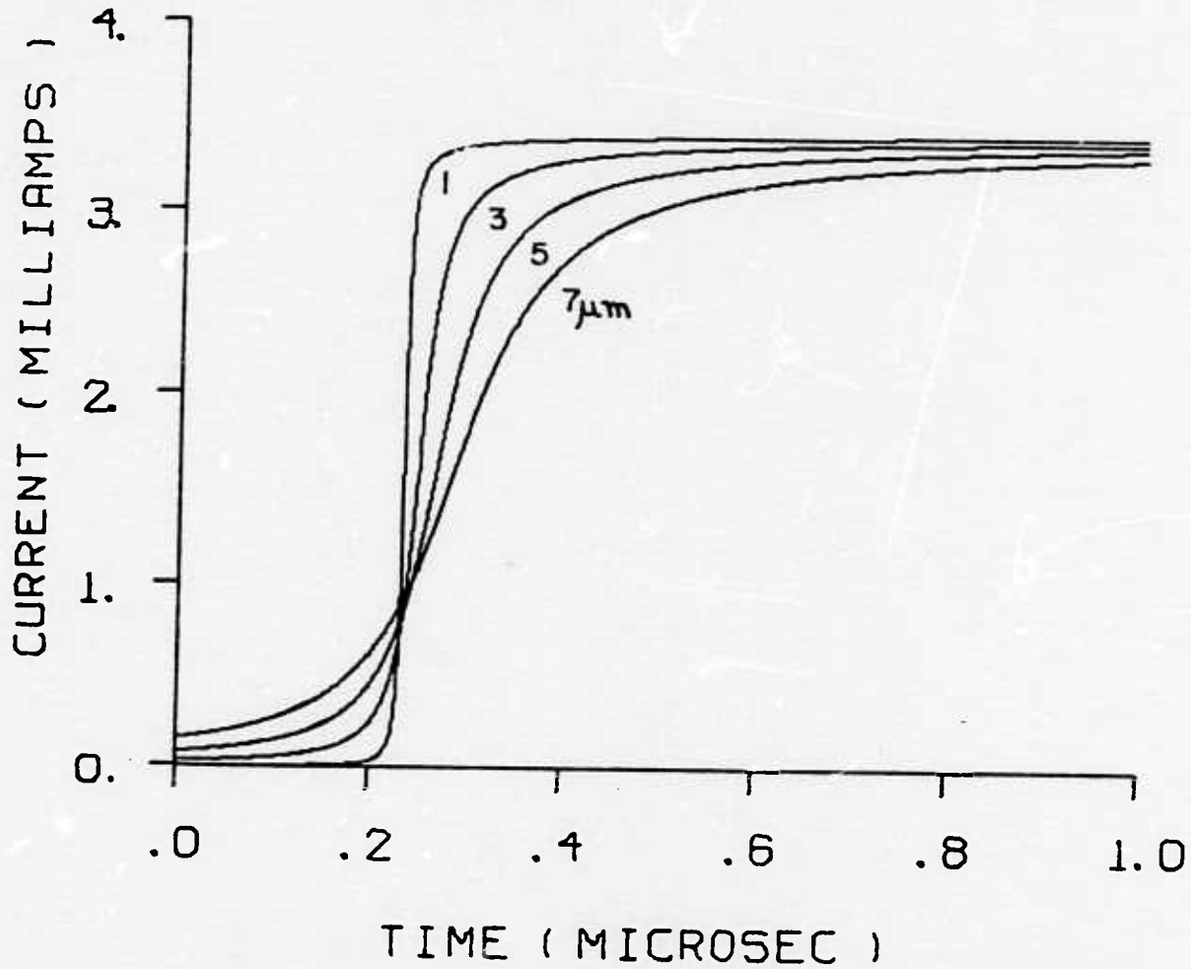

FIGURE 6. SIMULATED SWITCHING OF .13μm THICK As-Te FILM VARYING FILAMENT RADIUS.

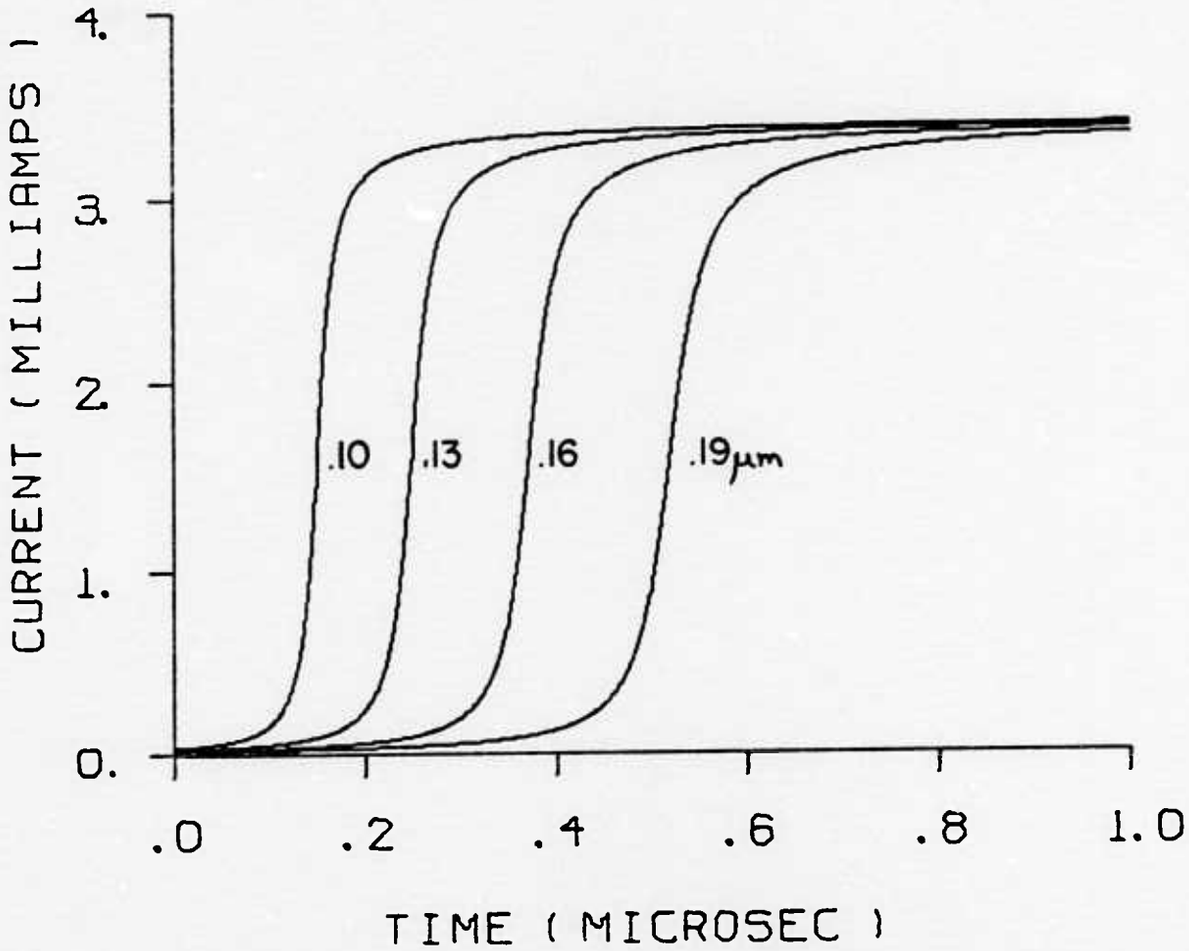

FIGURE 7. SIMULATED SWITCHING OF 3.μm RADIUS As-Te FILAMENT VARYING FILM THICKNESS.

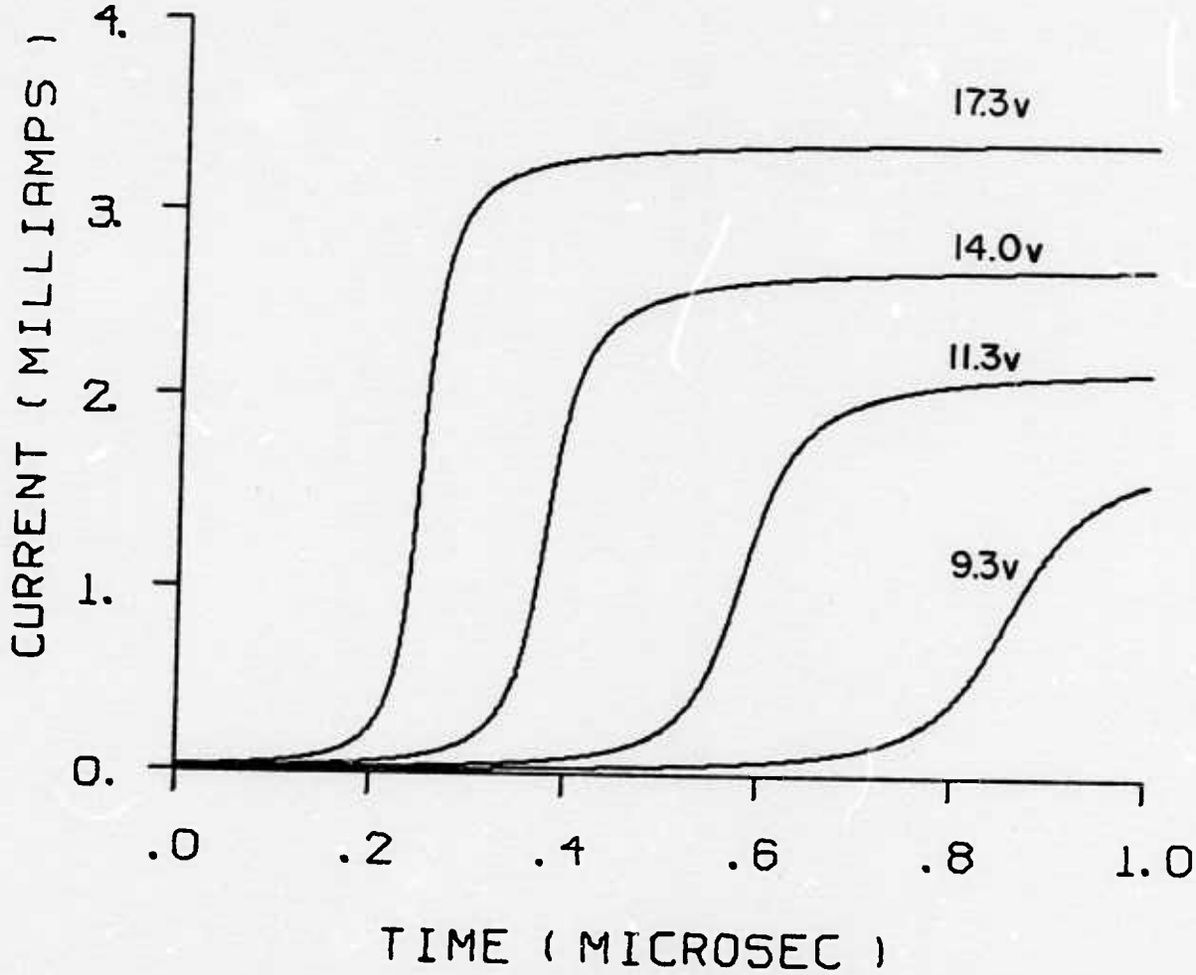

FIGURE 8. SIMULATED SWITCHING OF .13 μm THICK As-Te FILM WITH 3 μm FILAMENT RADIUS UNDER DIFFERENT APPLIED VOLTAGES.

Figure 9. SEM photograph of total device surface, stable device (200X).

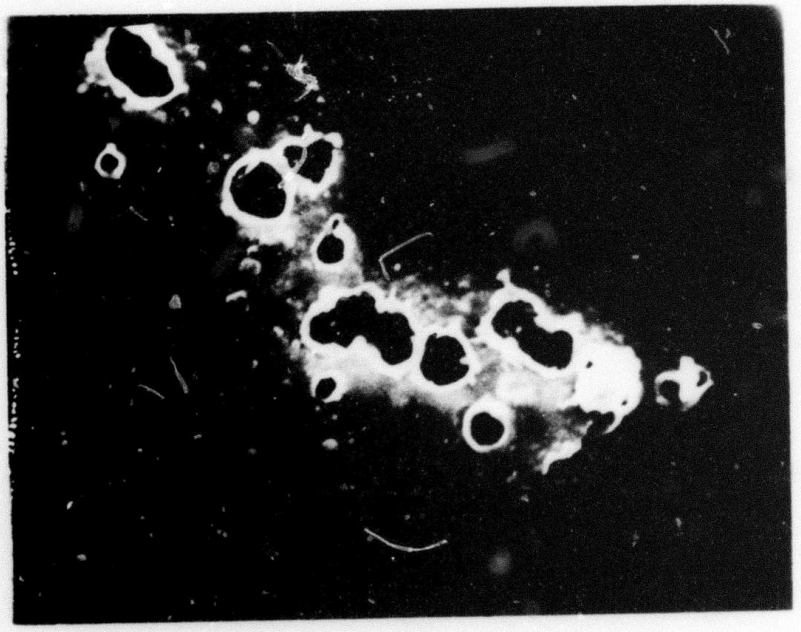

Figure 10. Closeup of Figure 9 (500X).

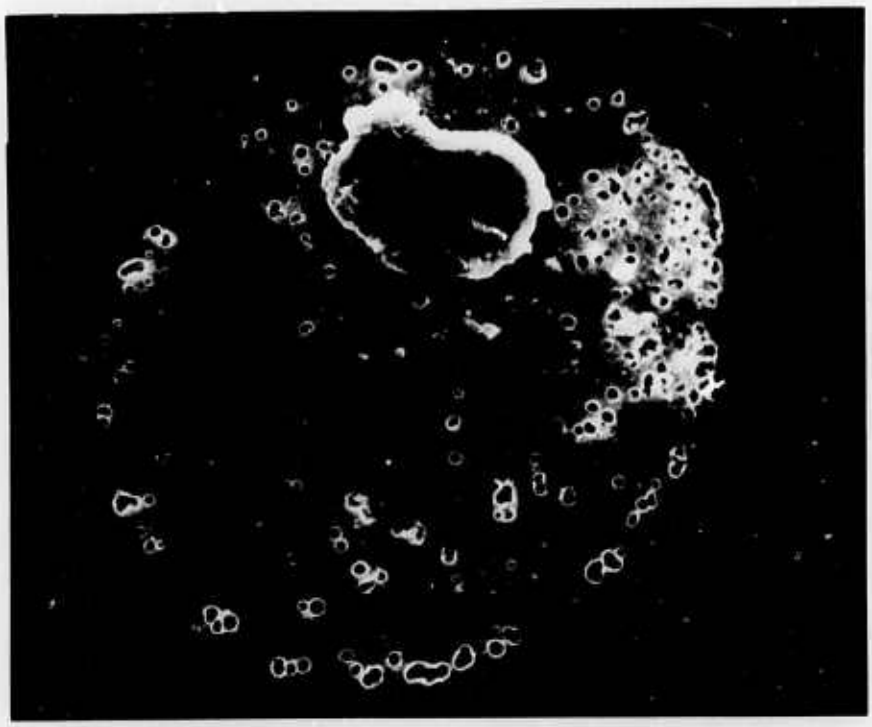

Figure 11. Portion of surface of unstable device (1000X).

Figure 12. Surface of device tested until failure (500X).

D. Discussion

The foregoing results suggest that switching characteristics are highly dependent on the size of the conducting region in the amorphous semiconductor. The following model is proposed, based on the radius of the conducting region, and is best understood by looking at three classes of filaments.

Class 1. The filament radius is extremely small (below approximately 2 μm).

Class 2. The filament radius is between approximately 2 and 10 μm.

Class 3. The filament radius is greater than approximately 10 μm.

Actually, the classes are based on the radius to thickness ratio but in our study to date we have used films having the same thickness, 2000 Å, so we express the variation in terms of radius only.

When a voltage is applied to a sample, one or more sites are more receptive to conduction than the whole sample. Initially, the smallest of these acts as the conduction filaments; however, for these very small filaments (Class 1), simulation has shown that temperatures high enough for vaporization are produced (see Table I). While these small filaments are being burned out, we would expect to see instability such as that shown in Figure 4. If this process continues, we eventually see total destruction as shown in Figure 12. If, on the other hand, Class 2 filaments form, we observe the stable switching shown in Figure 3. The areas in which pinholing occurs could be sites where initial burnout occurred before a filament with optimum radius was formed. All stable devices exhibited an initial instability before the onset of stable switching.

Occasionally, a device would not exhibit threshold switching; however, joule heating was observed with a rise time of perhaps five microseconds. This behavior would correspond to a Class 3 filament. The entire device was probably conducting uniformly with no individual filaments forming.

E. Summary and Conclusions

From the present investigation of switching phenomena in amorphous AsTe, the following conclusions can be made:

1. Conducting filaments of different sizes form by some random process.
2. These conducting filaments do not form by radial heat flow.
3. The filament radius controls the actual switching speed, while the film thickness controls the delay time before the onset of switching.
4. There exists an optimum size for the conducting filament which is approximately 3μ according to the simulation. A very large filament will transfer too much heat into the electrodes while a small one will overheat and vaporize.
5. In some cases, no stable filament ever forms resulting in the destruction of the entire conducting area.

F. Future Work

Work in the following areas is either planned or already underway:

1. Study of switching characteristics of higher melting materials in an effort to reduce instability.

2. Further characterization of switching using devices of different thickness as well as different applied voltages.
3. Further simulation of switching with additional studies of cooling and a more sophisticated combination of heating and cooling simulations.
4. More accurate measurement of film thickness using a stylus type measuring device.

Part II

ELECTRON SPECTRA OF CRYSTALLINE AND AMORPHOUS Si, Ge, AND AsTe

A. Introduction

As the parent elements of most semiconductor devices, silicon and germanium have been studied extensively. Their crystalline structure, thermal and electrical properties have been well characterized by numerous investigators.[1] With the advent of the first semiconductors and the band theory of semiconduction phenomena, it became apparent that new investigative techniques were necessary to experimentally determine the energy states of the electrons that participate in transport phenomena. The most successful of these techniques involve transmittance and reflectance in the infrared (0 ev-1.77 ev), visible (1.77 ev-3.1 ev) and ultraviolet (above 3.1 ev) regions of the energy spectrum.

In 1964 it was reported that there were differences in the optical properties of amorphous and crystalline germanium.[2] The reflectance spectra of Ge single crystals and epitaxially grown polycrystalline thin films showed strong reflectance peaks at 4.4 ev, 2.3 ev and 2.1 ev with shoulders at 2.5 ev and 3.3 ev. Amorphous films, prepared from the same source, did not show any structure over the same energy range. Subsequent investigation linked these differences to the loss of a sharp absorption edge in the electron density of states.[3-10] To qualitatively explain this behavior, several authors attempted to calculate the densities of electron states, taking into account the disorder inherent in amorphous solids.[6,11-14] Computed densities of states showed the same general features as the experimental densities of states, confirming the hypothesis that a sharp absorption edge in the valence band is characteristic of crystalline germanium and that the lack of a well defined absorption edge

in the same region is characteristic of amorphous germanium.

Theoreticians then broadened their calculations to include other materials such as Si, Se and SiO_2.[9,10,14-17] Their calculations indicated that the differences in optical properties observed for the crystalline and amorphous states of germanium should be common to all materials. This phenomenon has since been experimentally confirmed for Si.[18,19]

Gathering reflectance and transmission data to determine the densities of states in the I.R., U.V. and visible energy ranges is difficult, requiring various energy sources, detectors, diffraction gratings, data reduction using various mathematical models, and thin optically flat, self supporting films. High resolution electron spectrometers developed by Siegbahn and co-workers[20] have reduced the difficulties associated with spectrometric methods for determining the electron energy states in solids.

ESCA, Electron Spectroscopy for Chemical Analysis, is based on the well known photo-emission process. Electromagnetic radiation impinging on a material causes electrons, whose energy is less than that of the incident radiation, to be emitted. When the electrons are emitted into a vacuum chamber, 10^{-6} torr or better, which is compensated for the earth's magnetic field, the electron energies can be determined in an electron spectrometer. The result is directly proportional to the number of electrons occupying an arbitrary energy range, indicating that ESCA should be capable of directly determining the densities of states for energy ranges that would ordinarily require three sets of spectral data. In addition to the usual valence electron states, ESCA is also capable of resolving subvalence electron structure.

As a relatively new scientific tool, ESCA has shown a great deal of promise as a means for studying the chemical processes that occur at catalytic interfaces, the nature of the chemical bond,[21,22] and the band structure of elements and compounds.[23-30] The strength of ESCA stems from the fact that all electron levels, whose binding energy is less than that of the incident radiation, may be analyzed using a single nearly monochromatic energy source. It is limited by an inability to detect sparsely populated energy bands. However, the information obtained from ESCA should show essentially the same features as the densities of states obtained from composite I.R., visible and U.V. spectra.

The purposes of this paper are: (a) to ascertain whether there are differences in electron binding energy between amorphous and crystalline materials of the same composition, (b) to illustrate the experimental technique necessary to study occupied electron levels in the 0 ev-20 ev range of binding energy, (c) to show that the results are comparable to those obtained from other well established techniques, (d) to determine the specific differences between the crystalline and amorphous phases of a semiconducting glass system that exhibits both bi-stable and memory switching. To this end the experimental work has been divided into two segments: (1) studies of Ge and Si and (2) studies of AsTe. These materials were selected to illustrate that ESCA is capable of the precision necessary to yield the well established details of the densities of states, in crystalline and amorphous Ge and Si and to ascertain whether the same features exist in a switching glass composition.

B. Experimental

Samples of polycrystalline elements were prepared by cutting wafers 1 mm thick from high purity bulk ingots and laminating them to copper sample holders with a conducting, thermosetting silver epoxy. The thickness of the samples and the laminating adhesive were selected to eliminate any charging effects that might cause spurious peaks or peak shifts during analysis. After mounting, the samples were polished through 0.05 micron alumina, ultrasonicly cleaned in trichlorethylene and ethanol and selectively etched to remove the amorphous layers produced by polishing and any oxides formed during handling.

Amorphous samples of germanium and silicon were prepared by electron beam evaporation directly onto copper sample holders. The conditions of deposition were carefully controlled and nearly identical to those used by Spicer et al.[31] Thin film samples, 500A-1000A, were prepared fresh and transported to the ESCA analyzer in an inert atmosphere to reduce the possibility of oxide formation.

Polycrystalline samples of AsTe were prepared by reacting elements 99.99% pure in evacuated fused silica ampules for 12 hours at 650°C. The ampoules were quenched to 100°C in silicone oil and allowed to equilibrate for one hour, then heated to the crystalline temperature, 204°C, for ten minutes. Bulk ingots were then treated in the same way as the polycrystalline samples previously described. Dilute nitric acid was used as an etchant to remove the amorphous deformation layer created during polishing. Amorphous AsTe was prepared by sputtering, from electrodes prepared from bulk crystalline samples, directly onto cooled copper sample

holders. All amorphous AsTe samples were freshly prepared and transported to the electron analyzer in an inert atmosphere.

Aluminum $k\alpha_{1,2}$ x-radiation was used as an excitation source to photo-eject electrons from the samples. The electron emission was measured at 0.1 ev intervals over a 20 ev range. Data smoothing was accomplished by digitally fitting a moving five point parabola by the method of least squares. Calibration of the binding energy scale was accomplished using a gold standard and the procedure described by Baer et al.[27] Since an internal standard could significantly alter the electron spectra in the 0 ev-20 ev range, the strongest subvalence level in each kind of sample was standardized, using an internal standard and used to calibrate the outer energy ranges.

C. Results and Discussion

1. Subvalence levels of Ge and Si

The spectra of Ge 3d electrons (Figure 1) and Si 2p electrons (Figure 2) show that the peaks in the crystalline samples are shifted to higher binding energy than those of the amorphous samples by 0.1 ev, and crystalline samples show the initial formation of an oxide layer, probably located along high energy surfaces such as grain boundaries. Peak widths at half maximum of 1.6 ev for Ge and 1.4 ev for Si when compared to the natural line width at half maximum of Al $k\alpha_{1,2}$ x-radiation, 0.9 ev, indicates that there are probably two closely spaced peaks in each spectrum. Thus, the Ge peak actually corresponds to a $3d^{3/2}$ and $3d^{5/2}$ doublet and the Si peak corresponds

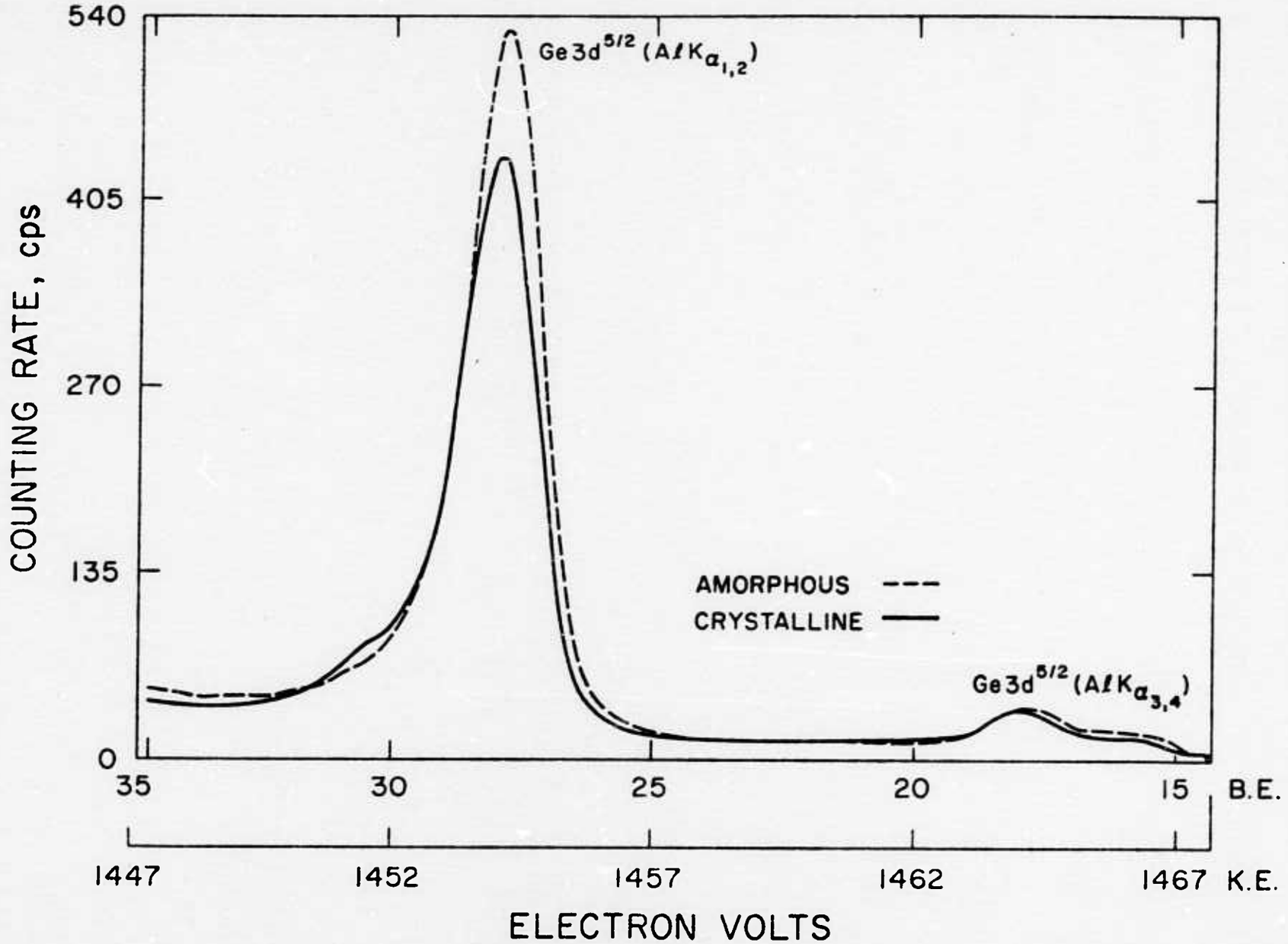

Figure 1. Electron spectra of the $3d^{5/2}$ electron levels in polycrystalline and amorphous germanium.

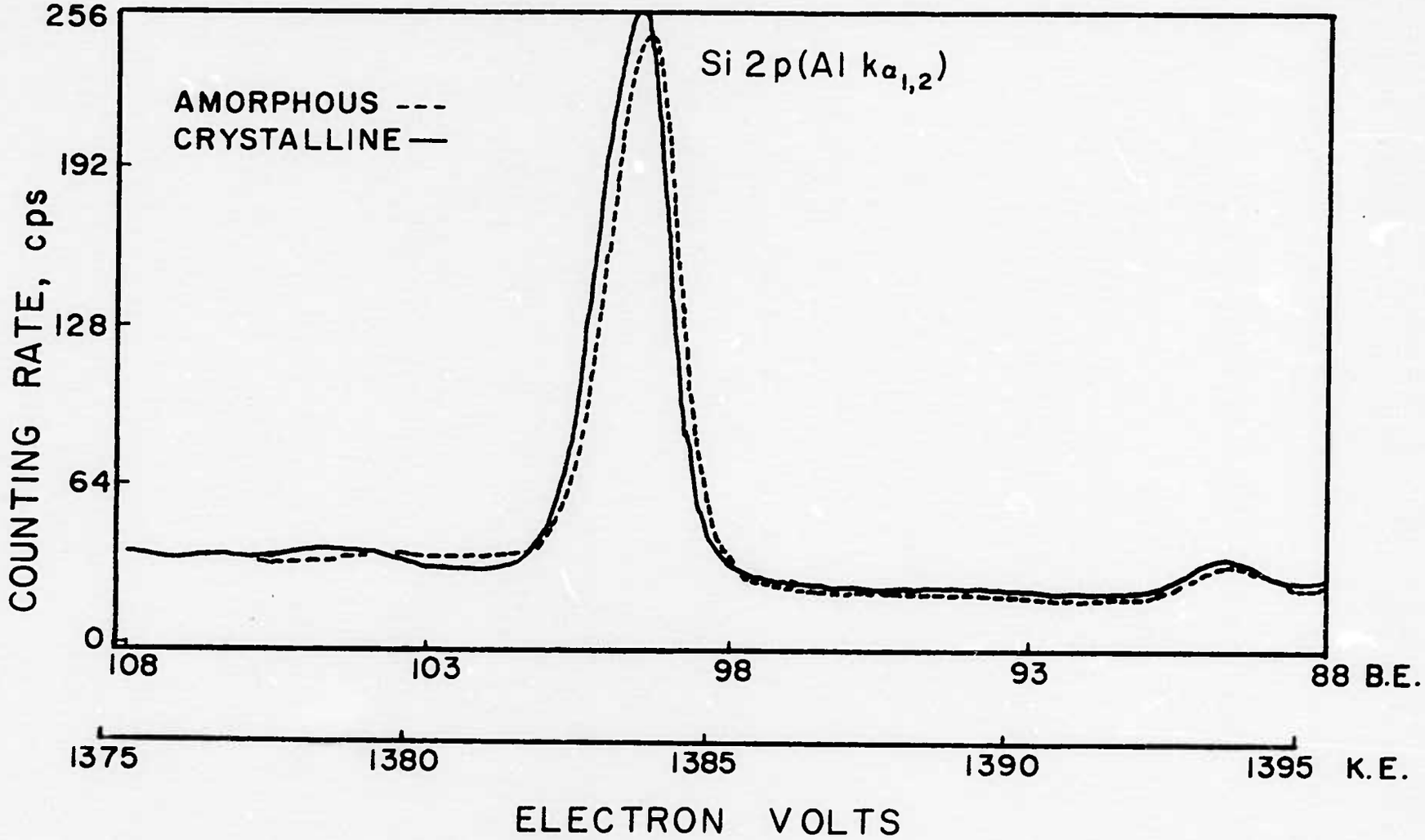

Figure 2. Electron spectra of the 2p electron levels in polycrystalline and amorphous silicon.

to a $2p^{1/2}$ and a $2p^{3/2}$ doublet. A slight skew to higher binding energy indicates that one peak in each doublet is less intense than the other. Siegbahn[20] has noted that the Si 2p levels are not resolved using $AlK\alpha_{1,2}$ x-radiation. However, spectral lines that occur as closely spaced doublets can be separated using numerical techniques.[25] Deconvolution of the Si 2p levels yield a 2:1 ratio of peak intensities, with the peaks separated by about 0.6 ev, the Si $2p^{3/2}$ being more intense than the Si $2p^{1/2}$. Similar results would be expected for Ge 3d levels since Ge 3d and Si 2p levels are nearly identical in shape. The additional broadening of the Ge peak could be the result of different peak intensity ratios or greater separation between the two peaks of the doublet.

2. Valence Electron Spectra of Ge and Si

Valence electron spectra for amorphous and crystalline germanium and silicon are shown in Figures 3 and 4. Crystalline spectra contain well defined peaks at 2.8 ev for Ge, and 3.1 ev for Si. These energy levels, corresponding to Ge 4p and Si 3p levels, are the least tightly bound electrons and as such probably participate in electron transport processes. The binding energy of the outermost occupied level of Si is 0.3 ev greater than for Ge as would be expected since Si is more resistive than Ge. The amorphous spectra resemble the crystalline spectra in that there are remnants of the Ge 4s and 4p levels and a reduction to very low noise levels near the zero of binding energy. They are notably different in that amorphous spectra do not have a well defined peak for binding energies less than 15 ev. This is the

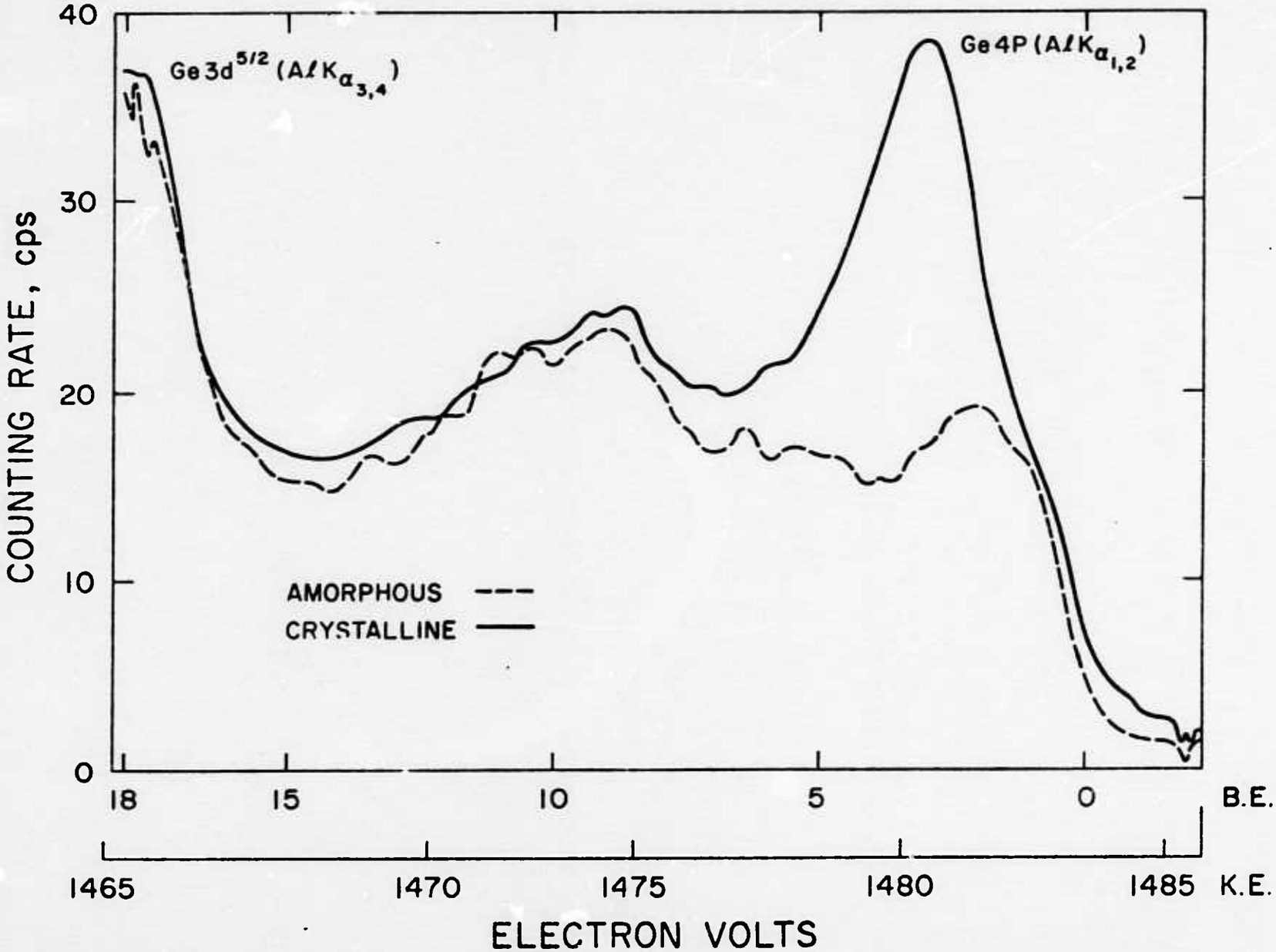

Figure 3. Electron spectra of the outer valence levels of polycrystalline and amorphous germanium.

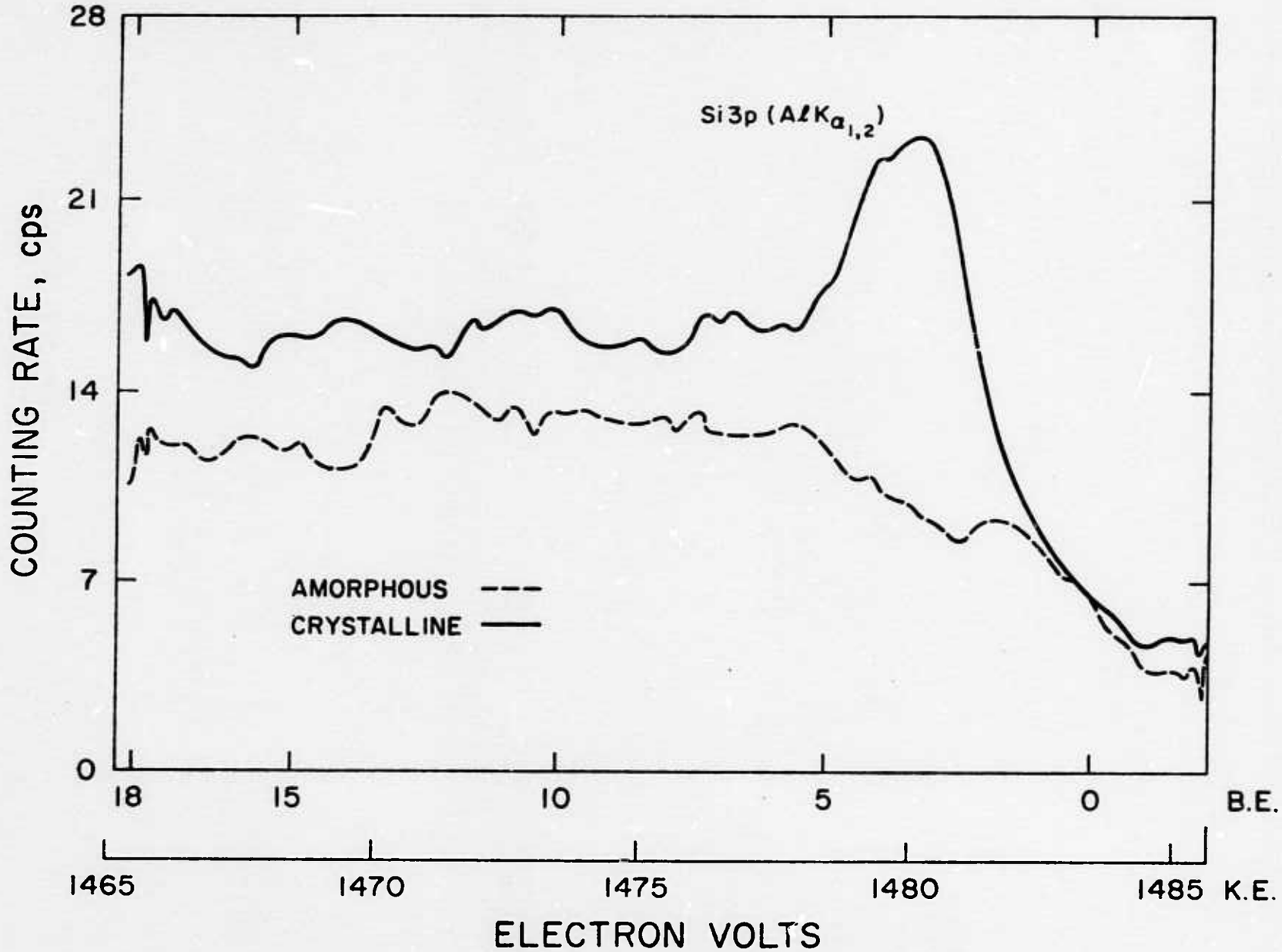

Figure 4. Electron spectra of the 3p valence electron levels in polycrystalline and amorphous silicon.

precise characteristic difference that is theoretically predicted by Kramer[15,16] and Jungk[14] and has been confirmed using optical spectroscopic techniques.[5,6]

Ley et al.[26] recently obtained valence level spectra of amorphous and crystalline silicon and germanium. Electron energy levels were located at 2.2 ev, 6.6 ev and 9.2 ev for silicon and 2.4 ev, 7.2 ev and 13.0 ev for germanium. For both elements, the higher energy peaks are taken to be s-like levels and the lower energy peak is taken to be p in character. The low energy peaks at 2.2 ev and 2.4 ev confirm our low energy peaks while the two s-like levels in germanium explain the structure located near 10 ev of binding energy in Figure 3. It is felt that the s-like levels found by Ley in the crystalline elements are the result of analyzing freshly cleaved surfaces prior to any oxidation.

3. Subvalence Electron Levels of Te

Spectra of the tellurium 3d levels in crystalline Te, crystalline As_2Te_3 and amorphous and crystalline AsTe are shown in Figure 5. The intensity scale is arbitrary and the base line displacements are chosen to emphasize the similarity of the spectra. There are no detectable peak shifts in the Te 3d levels when arsenic is combined with tellurium, nor is there any difference in peak width between amorphous and crystalline AsTe. The binding energies of the Te $3d^{3/2}$ and $3d^{5/2}$ electrons of 583.0 ev and 572.5 ev are comparable to those reported by other investigators.[20,32]

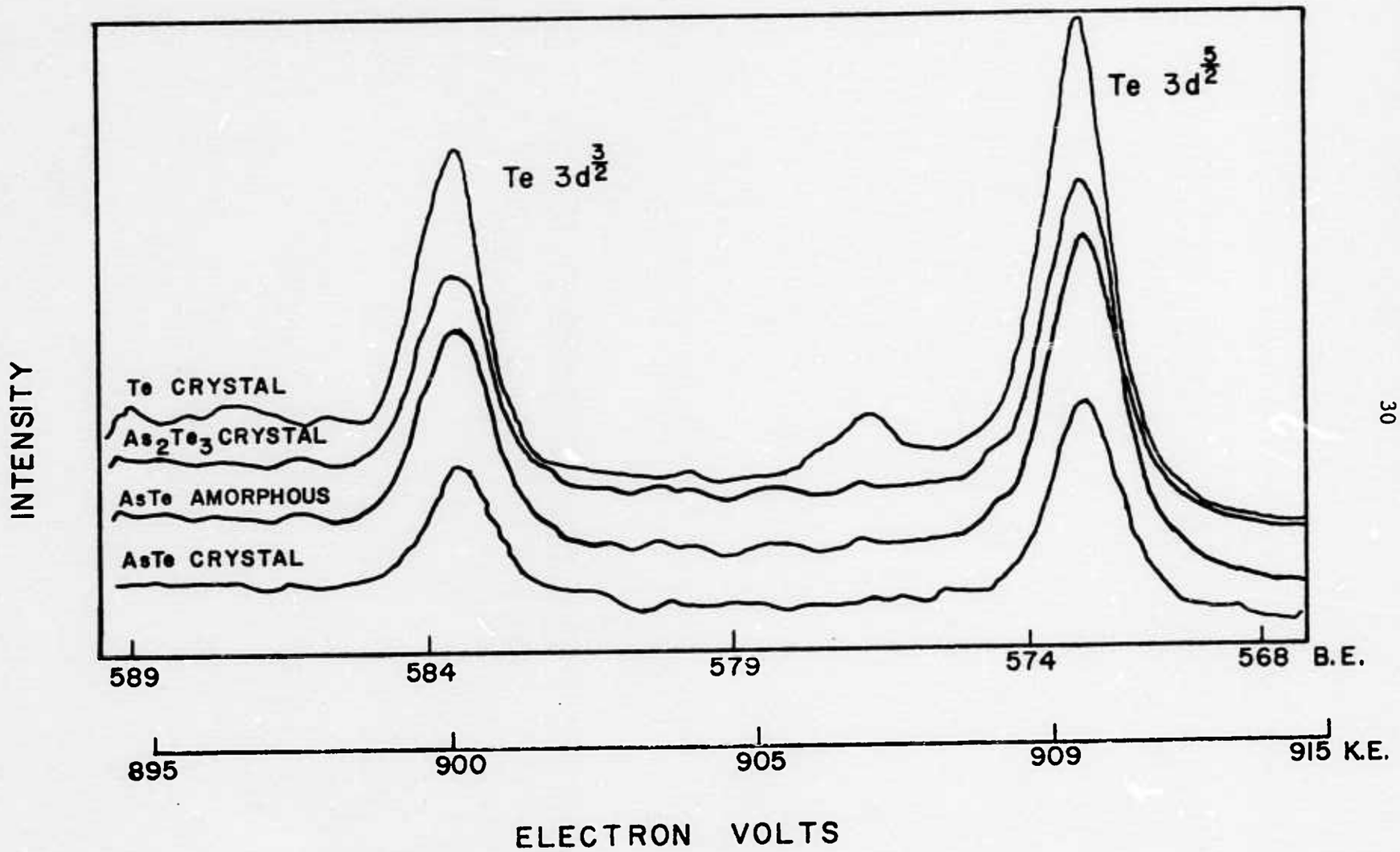

Figure 5. Tellurium 3d levels in crystalline Te, As_2Te_3, AsTe and amorphous AsTe.

Siegbahn[20] and Swartz[32] have shown that the binding energy shifts for all electron levels when two or more elements combine to form a compound and that the amount of shift is directly related to the degree of ionization of the bonds formed. Siegbahn[20] found that the amount of shift can be estimated using Pauling's electronegativity principle to calculate a modified oxidation number. Based on electronegativities, an As-Te bond would be 0.5% ionic resulting in a peak shift of less than 0.1 ev in complete agreement with the evidence of Figure 5. The absence of a chemical shift in the 3d electron levels of tellurium, the 0.5% ionic nature of the As-Te bond and the resistivity of crystalline As-Te mixtures (10^{-2} ohm cm) indicates that the As-Te bond is covalent.

4. Valence Electron Levels of AsTe

The densities of states for amorphous and crystalline AsTe are represented by Figure 6. The polycrystalline sample shows a shifted peak beginning at 7.3 ev and ending near zero ev with its center at 5.2 ev. Its half height width is 2.3 ev, indicating that it is a multiple peak whose average binding energy is greater than either the 4p levels of As (3 ev) or the 5p levels of Te (2 ev). However, the general shape indicates that there is a strong peak centered about 5.1 ev. The amorphous spectrum contains three peaks, two that are part of a doublet at 10.0 ev and 8.5 ev, and a broad peak extending from 15.8 ev to zero ev with its center at 2.9 ev and having a half height width of 4.8 ev. Such broadening could indicate several peaks whose individual peak widths are narrow compared to that of the

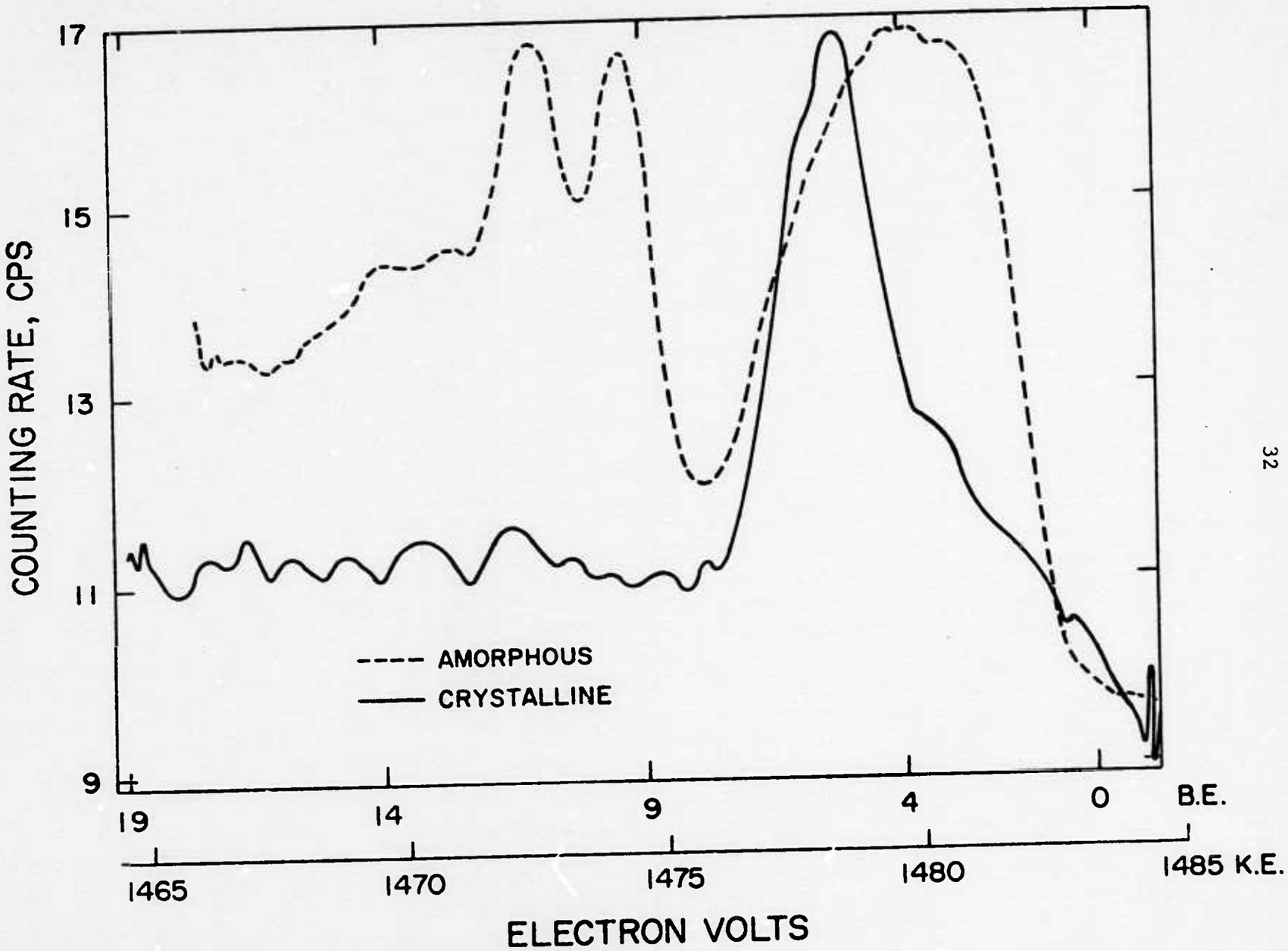

Figure 6. Valence level spectra of amorphous and polycrystalline AsTe.

incident radiation. This is similar to the phenomena noted for Si and Ge where the outer levels were reduced in intensity. The broadening is probably characteristic of semiconducting glasses.

Spectra of amorphous thin films, prepared by Ley et al.,[26] show the s-like valence levels of both amorphous Si and Ge to be merged and reduced in intensity while the p-like levels are essentially unchanged, with respect to the crystalline forms, except for a slight shift to lower binding energy. The data of Figures 3 and 4 show the p-like levels of both amorphous Si and Ge to be very much reduced in occupational density and shifted to lower binding energy. A possible explanation for the discrepancy may be found in the work of Thèye,[8] who showed that the optical properties of amorphous Ge are sensitive to crystallite formation and to heat treatment in the range 100°C to 300°C. Substantially, the same phenomena was observed by Brodsky[9] and Wihl[27] for amorphous Si films. Since the outermost bonding levels should be most effected by structural aberration resulting in a broadening of the energy bands that represent the s and p valence electron levels, it is believed that the films prepared by Ley et al.[26] must contain a significant number of microcrystallites.

D. Interpretation and Results

The current concept of the vitreous state indicates that atoms are tetrehedrally bonded, at normal crystalline band distances,[1,35] and that single tetrahedra share corners resulting in a random network of tetrahedrally coordinated atomic units. This concept would reduce the number of binding electrons in a given energy range, relative to the crystalline state, causing a reduction in intensity and a broadening of the electron densities of states.

This model differs from what would be expected from a vitreous model such as the one proposed by Tilton[34,35] which indicates that the basic structural unit of a vitreous substance is a tetrahedral arrangement of atoms that are themselves arranged in pentagonal duodecahedra. The simplest crystallite could contain as few as one duodecahedra composed of twenty tetrahedral units, having 15 axies of two-fold symmetry, 10 axies of three-fold symmetry, and 6 axies of five-fold symmetry. Crystallites may be bound together by sharing edges, faces, or corners. This model proposes a significant degree of crystallinity in amorphous solids. If this were the case, valence electron levels would be expected to remain sharp with possible broadening and a slight decrease in a solute intensity, indicative of a small degree of randomness in the structure. Examination of the electronic spectra of amorphous germanium and silicon does not reveal any structure in the valence levels that would support a vitreous model based on a random arrangement of crystallites. Thus, it is concluded that amorphous Si and Ge are probably composed of tetrahedral arrangements of atoms that are randomly arranged in a solid network.

This structural model is compatible with the structural interpretation of diffraction results by Turnbull and Polk[38] which indicates (a) that all nearest neighbor distances of the crystalline forms are preserved, (b) that dispersion in second neighbor distances is increased, and (c) that third neighbor distances are not detectable. Based on Turnbull and Polk's[38] analysis of diffraction results and the spectral data of Figures 3 and 4 for amorphous Ge and Si, the tendency of valence electrons to form sharp, well defined bands is probably most affected by the degree of ordering in second and higher atomic neighbors.

The broadening of electron energy bands indicates that new levels are occupied. These new levels, due to structural aberration, may be interpreted as dangling bonds and trapping levels resulting from deformed bonds. Conceivably, a sufficient number of new levels with widely varying energies could result in dispersing the energy band to the extent that no single level is dense enough to be detected. If one accepts this explanation, then it becomes apparent that electron transport processes should be described by an electron transport model similar to the one proposed by Anderson.[39] This model assumes a three-dimensional array of potential wells of random depth spread over an energy range V_o. By letting Δ be the energy that would exist if the ground states of an identical array of wells at some average energy were allowed to overlap to form a band, Anderson was able to calculate a finite ratio V_o/Δ above which an electron would not be able to diffuse away from its potential well. Mott[40] postulated that for a low density of potential wells that localization of the electron states would give rise to a sharp band edge in amorphous

electronic conductors. However, Cohen, Fritzsche and Ovshinsky[41] suggested that there is a high density of potential wells in electronic amorphous conductors and as a result, the localized electron levels have overlapping tails in the densities of states.

The data of Figures 3 and 4 show that the 4p levels of amorphous germanium and the 3p levels of silicon are so sparsely populated that they are nearly indetectable. Since there are no significant shifts in the binding energies of the subvalence levels of amorphous germanium and silicon, relative to their crystalline phases, then the atoms are not ionized indicating that the 4p level of Ge and the 3p level of Si have been broadened rather than removed. A comparison of conductivities reveals that at room temperature the crystalline phase is two to four orders of magnitude more conducting than the amorphous phase. Similarly, the amorphous spectra of AsTe (Figure 6) shows a broadened outer valence level and the crystalline phase exhibits a conductivity, at room temperature, that is greater by a factor of 10^6 [42] than the conductivity of the amorphous phase. These observations indicate that, (a) the outer valence levels are responsible for electrical transport processes, (b) broadened valence levels are characteristic of the amorphous materials studied, and (c) the valence electrons are strongly localized.

E. Conclusions

1. The lack of a significant shift in the binding energy of subvalence levels indicates that the bond type in the materials studied is the same for both the crystalline and amorphous states.
2. Broadening of the valence band in amorphous materials relative to the valence band in crystalline materials is characteristic of the amorphous state.
3. Valence band electrons are largely responsible for the electron controlled processes studied. In particular, the 4p electrons of Ge and the 3p electrons of Si are responsible for electronic conduction processes.
4. The valence band electrons are strongly localized in amorphous Si, Ge and AsTe.
5. The As-Te bond is covalent.
6. X-Ray electron spectroscopy is superior to conventional techniques for studying the electron spectra of solid materials since:
   a) only one sample is required,
   b) the sample is small and relatively easy to prepare,
   c) only one energy source and only one detector are required to study the valence and subvalence electron levels, and
   d) all energy levels may be studied simultaneously.

F. Future Work

A continuation of this work is expected to focus on the bonding and valence electron levels of other semiconducting glass compositions that exhibit both memory and non-memory switching. Utilization of an yttrium source in the ESCA system is expected to improve the resolution of valence electron spectra.

References

1. Adler, David, CRC Critical Reviews in Solid State Sciences (1971).

2. Donovan, T. M., Ashley, E. J., J. Opt. Soc. Am. 54, 1141 (1964).

3. Tauc, J., Grigorovici, R., and Vancu, A., Phys. Stat. Sol. 15, 627 (1967).

4. Wales, J., Lovitt, G. J., and Hill, R. A., Thin Solid Films, 1, 137 (1967).

5. Donovan, T. M. and Spicer, W. E., Phys. Rev. Let. 21, 1572 (1968).

6. Donovan, T. M., Spicer, W. E., Bennett, J. M. and Ashley, E. J., Phys. Rev. B, 2, 397 (1970).

7. Tauc, J., Abraham, A., Zallen, R., and Slade, M., J. Non. Cryst. Solids 4, 233 (1970).

8. Thèye, M. L., Mat. Res. Bull., 6, 103 (1971).

9. Brodsky, M. H., J. Sci. and Vac. Tech., 8, 1, 125 (1971).

10. Kramer, B., Phys. Stat. Sol. (b), 47, 501 (1971).

11. Gubanov, A. I., Quantum Electron Theory of Amorphous Conductors, Consultants Bureau Enterprises, Inc., New York (1965).

12. Mott, N. F., Advan. Phys., 16, 1 (1967).

13. Mott, N. F., Contemp. Phys., 10, 125 (1969).

14. Jungk, G., Phys. Stat. Sol. (b), 46, 603 (1971)

15. Kramer, B., Phys. Stat. Sol., 41, 725 (1960).

16. Kramer, B., Maschke, K., Thomas, P., Treusck, Jl, Phys. Rev. Let., 25, k5m k020 (1970).

17. Bennett, A. J., Roth, L. M., Phys. Rev. B. 4, 8, 2686 (1971).

18. Philipp, H. R., J. Phys. Chem. Solids, 32, 1935 (1971).

19. Brown, F. C., Rustgi, O. P., Phys. Rev. Let. 28, 8, 497 (1972).

20. Siegbahn, Kai, et al., Electron Spectroscopy for Chemical Analysis, University of Uppsala, Uppsala, Sweden (1968).

21. Betteridge, D., Analytical Chemistry, 44, 5, 100R (1972).

22. Hercules, David M., Analytical Chemistry, 44, 5, 106R (1972).

23. Hagstrom, S., Nordling, C., and Siegbahn, K., Phys. Let., 9, 3, 235 (1964).

24. Fadley, C. S., Shirley, D. A., Phys. Rev. Let., 21. 14, 980 (1968).

25. Fadley, C. S. and Shirley, D. A., J. Res. Nat. Bur. Stds. A. Phys. and Chem., 74A, 543 (1969).

26. Ley, L., Kowalczyk, S., Pollak, R., and Shirley, D. A., Phys. Rev. Let., 29, 16, 1088-1092 (1972).

27. Wihl, M., Cardona, M., and Tauc, J., J. Non. Cryst. Solids, 8-10, 172-178 (1972).

28. Novakov, T., Phys. Rev. B., 3, 8, 2693 (1970).

29. Baer, Y., Heden, P. F., Hedman, J., Klasson, M., Nording, C., and Siegbahn, K., Physica Scripta, 1, 55 (1970).

30. Sharma, J., Staley, R. H., Rimstidt, J. D., Fair, H. D., and Gora, T. F., Chem. Phys. Let., 9, 6, 564 (1971).

31. Thomas, J. M., Evans, E. L., Barber, M., and Swift, P., Trans. Faraday Soc., 67, 1875 (1971).

32. Kono, S., Ishii, T., Sagawa, T., and Kobayasi, T., Phys. Rev. Let., 28, 21, 1385 (1972).

33. Spicer, W. E., Donovan, T. M., and Fischer, J. E., J. Non. Cryst. Solids, 8-10, 122-127 (1972).

34. Swartz, W. E., X-Ray Photoelectron Spectroscopic Studies of Phosphorous, Nitrogen, Selenium, Tellurium and Molybdenum Compounds, Ph.D., Thesis, M.I.T. (1971).

35. National Academy of Sciences, Fundamentals of Amorphous Semiconductors, Nat. Acad. of Sci. (1972).

36. Tilton, L. W., J. Res. Nat. Bur. Stds., 59, 2, 139-154 (1957).

37. Tilton, L. W., J. Res. Nat. Bur. Stds., 60, 4, 351-364 (1958).

38. Turnbull, D. and Polk, D. E., J. Non. Cryst. Solids, 8-10, 19-35 (1972).

39. Anderson, P. W., Physical Review, 109, 5, 1492 (1958).

40. Mott, N. F., Phil. Mag., 13, 989, 1966, Adv. Phys., 16, 49 (1967), Phil. Mag., 17, 1259 (1968).

41. Cohen, M. H., Fritzche, H., and Ovshinsky, S. R., Phys. Rev. Let., 22, 1065 (1969).

42. Eusner, P. R., Durden, L. R., and Slack, L. H., J. Am. Ceram. Soc., 55, 1, 43 (1972).

43. Shaw, M. P., Moss, S. C., Kostylev, S. A., and Slack, L. H., Preswitching and Postswitching Phenomena in Amorphous Semiconducting Films, Appl. Phys. Lett. 22 (3) 114-117 (1973).